Comparison of (non)-sulfided NiNaY zeolite catalysts prepared by ion-exchange and impregnation by xenon adsorption and ^{129}Xe NMR

T.I. Korányi [1], L.J.M. van de Ven, W.J.J. Welters, J.W. de Haan, V.H.J. de Beer and R.A. van Santen

Schuit Institute of Catalysis, Eindhoven University of Technology, PO Box 513, 5600 MB Eindhoven, The Netherlands

Received 24 June 1992; accepted 6 October 1992

Ni^{2+} exchanged and $NiCl_2$ impregnated non-sulfided and sulfided NaY zeolites were characterized by xenon adsorption isotherms, ^{129} Xe NMR and thiophene hydrodesulfurization. The nickel species are located mainly inside the micropores of the zeolites in all samples. Ion-exchange results in a more homogeneous distribution of these species than impregnation. This explains their lower hydrodesulfurization activity compared to the ion-exchanged samples.

Keywords: Xenon adsorption; ^{129}Xe NMR; zeolites; NiNaY, sulfidation of; hydrodesulfurization (HDS); thiophene

1. Introduction

Sulfided NiNaY zeolites are active in hydrodesulfurization and hydrocracking catalysis. In order to understand their catalytic behaviour it is important to determine the amount and location of the transition metal species inside the zeolite structure. One possibility is to probe the presence of nickel compounds inside the zeolite cages by ^{129}Xe nuclear magnetic resonance (NMR) chemical shifts of xenon adsorbed in the micropores of zeolites [1]. Another one is to study the xenon adsorption isotherms and isosteric heat of adsorption of xenon.

NiNaY zeolites prepared by ion-exchange of NaY precursors using nickel nitrate have been studied before by the xenon NMR technique in their calcined [2,3] and reduced [4] states. The earlier results indicated that above 14% exchange of the sodium by nickel ions the supercage sites of NiNaY zeolites

[1] On leave of absence from the Institute of Isotopes, Budapest, Hungary.

were occupied by hydrated and dehydrated nickel ions [4]. It was suggested that most of the nickel ions migrated to positions outside of the supercages due to long (12 h) and high (623 K or higher) temperature treatment in vacuum [2] or reduction in hydrogen at 643 K for 3 h [4].

Preliminary results from our laboratory obtained with sulfided NiNaY zeolites prepared by ion-exchange indicate that the (2–8 wt%) nickel can be completely sulfided to Ni_3S_2-like clusters (EXAFS and TPS [5]), that are located mainly inside the zeolitic structure (Xe NMR [5,6]). Whereas the exact supercage diameters of the NiNaY samples prepared by ion-exchange could not be evaluated from the xenon NMR data using either the model of Fraissard and co-workers [7,8] or that of Derouane et al. [9–13], the results indicated that the nickel was completely and homogeneously sulfided and the sulfide phase was mainly situated inside the zeolitic structure. The small nickel sulfide clusters appeared efficient in thiophene hydrodesulfurization [5,6].

In the present study the attention will be focussed on the determination of the sulfide distribution of ion-exchanged and impregnated samples using the two methods mentioned above, i.e. xenon NMR chemical shifts and xenon adsorption isotherms.

2. Experimental

2.1. PREPARATION AND PRETREATMENT OF SAMPLES

NaY zeolite ($Na_{56}(AlO_2)_{56}(SiO_2)_{136}(H_2O)_{250}$ LZY-52 Akzo Chemie Ketjen) samples were ion-exchanged by $NiCl_2$ solutions stirred at room temperature for 24 h. After filtration the zeolites were washed until the filtrate was Cl^- free (checked by $AgNO_3$) and they were dried at 380 K in air overnight.

Another NaY zeolite ($Na_{53}(AlO_2)_{53}(SiO_2)_{139}(H_2O)_{235}$ CLA Ketjen) was impregnated by $NiCl_2$ solutions. After drying at 380 K in air overnight the impregnated zeolites were calcined at 673 K in air for 2 h. The dried ion-exchanged (I-E) and calcined impregnated (IMP) samples were stored above a saturated $CaCl_2$ solution in order to stabilize their weight. The catalysts were pressed, crushed and sieved. The 125–425 μm fraction was used for xenon adsorption, Xe NMR and thiophene HDS activity tests. The composition of the above samples was checked by atomic absorption spectroscopy (AAS). The catalyst notation used in this paper is shown in table 1.

A mass of 0.8–1.5 g zeolite was loaded into a flow reactor. Heating to 673 K at a rate of 6 K/min and holding this temperature for 2 h either in a He stream or in a mixture of 10% H_2S in H_2 (60 ml/min) resulted in the non-sulfided, oxidic (O) and the sulfided (S) samples, respectively. The water loss during this treatment in helium (determined gravimetrically) was very similar for all oxidic

Table 1
Designation, composition and water content of oxidic (Ni)NaY zeolite samples

Sample	NaY	I-E2	I-E4	I-E6	I-E8	IMP2	IMP4	IMP6
Ni content [a] (wt%)	0	1.9	3.7	5.7	7.6	2.0	3.8	5.5
water loss [b] (wt%)	25.0	25.4	25.5	25.8	26.2	22.7	22.1	21.5

[a] Determined by AAS.
[b] During heating up to and keeping at 673 for 3 h in helium.

samples (table 1). From the EXAFS and TPS results [5] we can propose that the nickel is completely sulfided during the treatment in H_2S/H_2.

2.2. XENON ADSORPTION AND NMR

In order to avoid contact with air and water the pretreated samples were transferred into the NMR tubes using a recirculation type glove box (oxygen and water content lower than 2 ppm). The samples were evacuated at room temperature to a pressure below 10^{-4} mbar and stored in a volumetric, grease-free adsorption apparatus. Xenon was adsorbed on these samples at 303, 296 and 273 K. The density of adsorbed Xe is expressed as mol xenon / kg zeolite (n/m). The Xe adsorption heats are calculated from the slope of $\log p - 1000/T$ curves of the isotherms using the Clausius–Clapeyron equation [14]. The NMR spectra of adsorbed xenon were taken at 303 K on a Bruker CXP 300 Fourier transform instrument at 83 MHz with pulse excitation (0.5 s pulse delay) on stationary samples. The number of scans was between 10^2 and 10^5.

2.3. ACTIVITY MEASUREMENTS

Activity tests for thiophene hydrodesulfurization (HDS) test reactions were carried out over the sulfided zeolites (250 mg) in a flow reactor (1 bar, 673 K) using a mixture of 4 vol% thiophene in H_2 (60 ml/min). The sulfidation conditions were the same as described in section 2.1. The catalytic activities are expressed in reaction rate constants k calculated from the absolute conversion of thiophene. Initial activities (after 5 min run time) were used for comparison of the samples because of strong deactivation of the catalysts.

3. Results

The xenon adsorption isotherms of NaY and I-E samples (fig. 1) show an almost linear increase with increasing pressure, and those of oxidic (O) as well as NaYS and I-E2S zeolites are very close to each other. The isotherms of I-E4S, I-E6S, and I-E8S samples show a decreasing adsorption capacity for

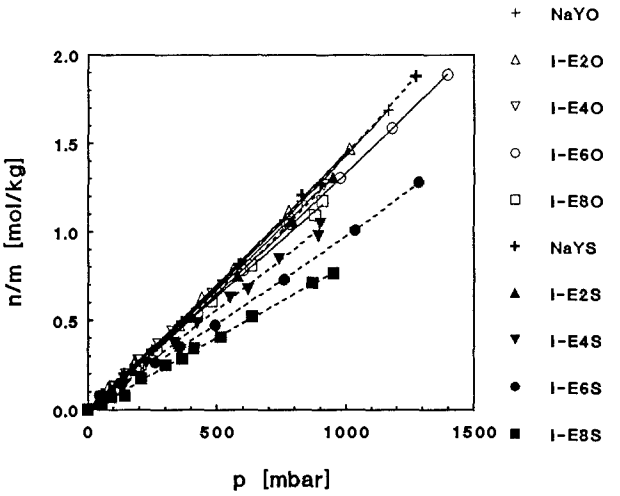

Fig. 1. Isotherms for xenon adsorbed on NaY and NiNaY zeolites ($T = 303$ K) prepared by ion-exchange.

xenon in this order and there is a slight saturation effect with increasing xenon pressure.

The adsorption isotherms of NaY and IMP zeolites (fig. 2) are also identical up to 2% nickel loading, but contrary to the I-E samples, not only the sulfided, but also the oxidic zeolites show a decreasing xenon adsorption capacity at 4 and 6% nickel content. The isotherms of oxidic and sulfided zeolites are the same at identical nickel loadings.

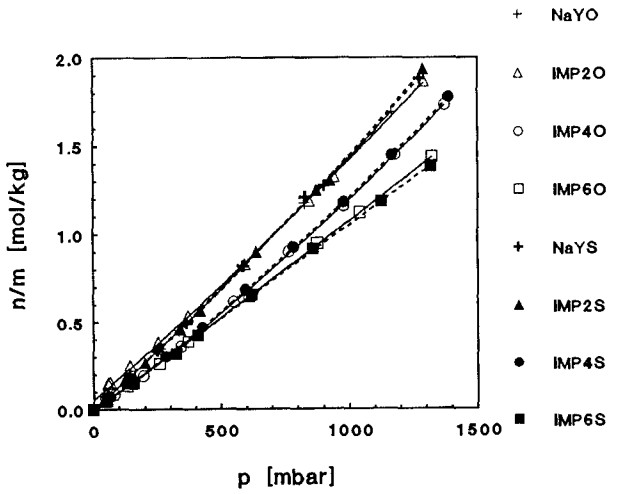

Fig. 2. Isotherms for xenon adsorbed on NaY and Ni/NaY zeolites ($T = 303$ K) prepared by impregnation.

Table 2
Isosteric adsorption heats of xenon (Q) and ^{129}Xe NMR characteristics of oxidic (upper part) and sulfided (lower part) (Ni)NaY zeolites

Sample	NaY	I-E2	I-E4	I-E6	I-E8	IMP2	IMP4	IMP6
oxidic								
Q_O (kJ/mol)	21.1	–	–	21.3	–	22.6	22.5	22.3
FWHH [a] (ppm)	2	4.5	8	13	23	7	17	32
δ_{-1} [b]	–	0.01	0.33	−0.12	0.61	0.14	0.22	0.16 [c]
δ_0 [b] (ppm)	59.1	68.8	71.3	80.5	93.4	83.8	108.7	137.6 [c]
δ_1 [b]	22.9	22.9	25.2	23.3	33.1	19.2	15.8	−4.0 [c]
sulfided								
Q_S (kJ/mol)	20.9	20.1	21.4	23.0	23.2	19.8	21.6	21.8
FWHH [a] (ppm)	2	1.5	3.5	4.5	6	3	3	4
δ_{-1} [b]	–	0.04	−0.03	0.05	0.21	−0.08	−0.09	0.12
δ_0 [b] (ppm)	61.0	60.6	67.9	71.1	75.3	64.0	64.8	65.2
δ_1 [b]	22.3	23.5	24.4	26.4	31.3	20.9	22.8	28.1

[a] Full width at half height of Xe NMR peak at $n/m = 0.5$.
[b] Parameters in eq. (1), calculated from the Xe NMR shift curves.
[c] Parameters obtained by fitting including the three-body Xe–Xe collision term (δ_2).

The isosteric heats of xenon adsorption (Q_O and Q_S) are shown in table 2. Those of oxidic samples are similar to each other within the same series (I-E or IMP). The isosteric adsorption heats of sulfided ion-exchanged zeolites increase with increasing nickel loading, but those of impregnated samples are essentially the same (IMP4S and IMP6S) or significantly smaller than the others (IMP2S 19.8 kJ/mol).

All samples show a single Xe NMR peak. The peak width (FWHH) increases with increasing nickel content, particularly in the case of oxidic zeolites (table 2). The NMR peak width of sulfided samples is much smaller than that of their oxidic counterparts (table 2).

The Xe NMR chemical shifts as functions of adsorbed xenon densities are shown in figs. 3–6. The shifts of all (Ni)NaY samples (except IMP6O at low density, see fig. 5) increase with increasing amount of adsorbed xenon. The experimental data shown in figs. 3–6 can be fitted by the Fraissard–Cheung equation [3,15],

$$\delta = \delta_{-1} d^{-1} + \delta_0 + \delta_1 d + \delta_2 d^2, \tag{1}$$

where d is the local density of xenon atoms (n/m) adsorbed in the pores. δ_0 is the sum of density-independent terms including chemical shifts due to Xe–wall, Xe–adsorbate and Xe–electric field gradient interactions. The term $\delta_{-1} d^{-1}$ represents the nonlinear electromagnetic or adsorption effect, whereas δ_1 and δ_2 arise from binary (or two-body) and ternary (or three-body) Xe–Xe collisions, respectively. Fitting the experimental data shown in figs. 3–6 with eq. (1) results in oscillating δ_1 values and the two- and three-body Xe–Xe collision parameters

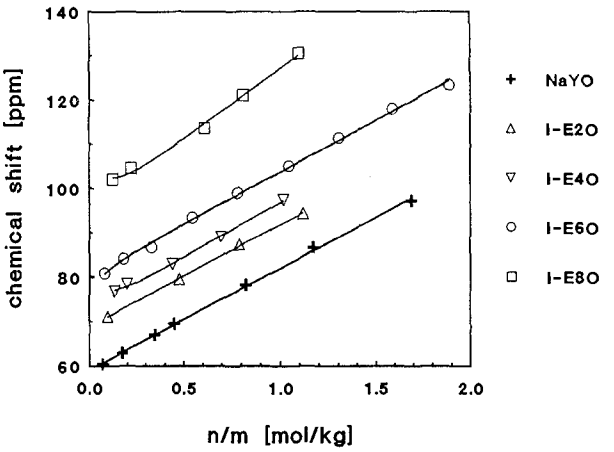

Fig. 3. ^{129}Xe NMR chemical shifts as a function of the xenon density (mol/kg) adsorbed on oxidic ion-exchanged (Ni)NaY.

(δ_1 and δ_2) do not change in parallel. Neglecting the $\delta_2 d^2$ term in eq. (1) gives the best regression (except IMP6O), better standard deviation of the data is gained than in linear fitting (except NaYO and NaYS). The results of this fitting are shown in table 2. The adsorption constant (δ_{-1}) of the I-E8O sample is remarkably high. This reflects the effect of the electric field gradients of bare Ni^{2+} ions to the adsorbed xenon atoms. The intercepts (δ_0) increase with increasing nickel loading particularly in the case of oxidic impregnated zeolites (fig. 7).

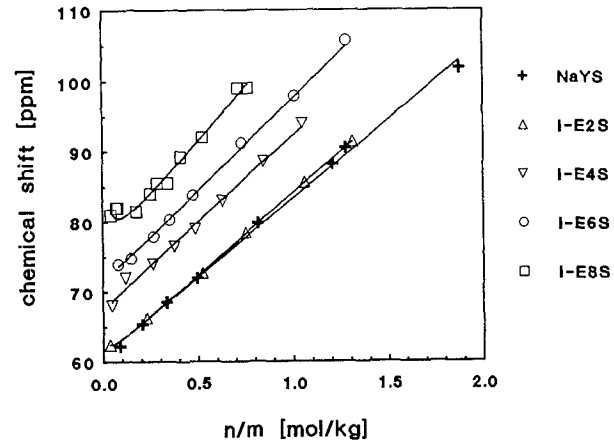

Fig. 4. ^{129}Xe NMR chemical shifts as a function of the xenon density (mol/kg) adsorbed on sulfided ion-exchanged (Ni)NaY.

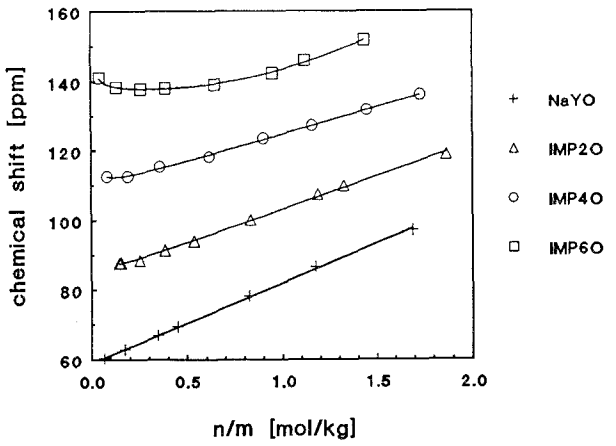

Fig. 5. ^{129}Xe NMR chemical shifts as a function of the xenon density (mol/kg) adsorbed on oxidic impregnated (Ni)NaY.

The initial HDS activity of sulfided catalysts (fig. 8) increases linearly with the nickel content. The initial activities of I-E zeolites are higher than those of IMP samples, but the former catalysts become deactivated faster than the latter.

4. Discussion

The NMR signal of adsorbed xenon reflects the average of various Xe positions and interactions, because the exchange of xenon between the different positions in the zeolite is fast on the NMR timescale [1,16]. Due to the relatively large diameter of the xenon atom ($D_{Xe} = 4.37$ Å) information is only obtained

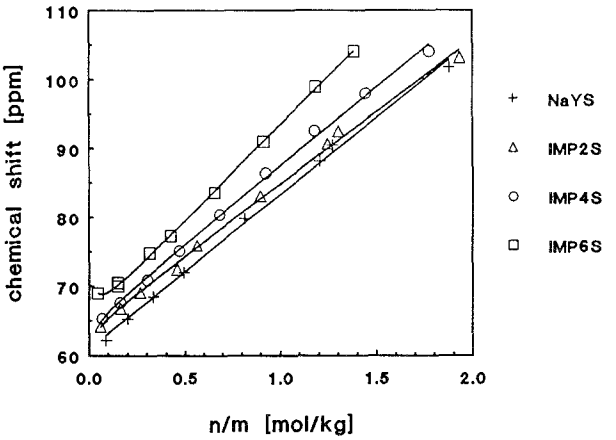

Fig. 6. ^{129}Xe NMR chemical shifts as a function of the xenon density (mol/kg) adsorbed on sulfided impregnated (Ni)NaY.

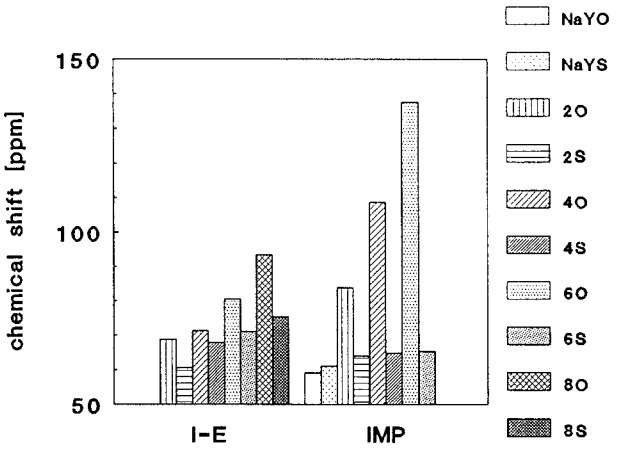

Fig. 7. ^{129}Xe NMR chemical shifts extrapolated to zero xenon density (δ_0) of (Ni)NaY.

on the larger pores, e.g., on the supercages, but not on the sodalite cages of faujasite type (NaY) zeolites [1].

NaY has a single, narrow Xe NMR peak (table 2) and exhibits linear chemical shift plots (figs. 3–6 and table 2) indicating the homogeneity of cages and channels and the lack of paramagnetic cations in the zeolite structure in accordance with the results obtained by Ito and Fraissard [17].

In the case of NiNaY zeolites the spectrum of adsorbed xenon consists of a single line, but the NMR peak widths are larger than for NaY (see FWHH values in table 2) and a slight concave curvature has been found in the NMR shift plots (figs. 3–6) in accordance with the literature [2,3,17]. It is worth noting that NaYS is not sulfided under the applied condition, NaYS means NaY zeolite treated by H_2S/H_2. The wide peak width of oxidic samples shows the inhomogeneity of the cage walls [16] due to the variety of hydrated nickel

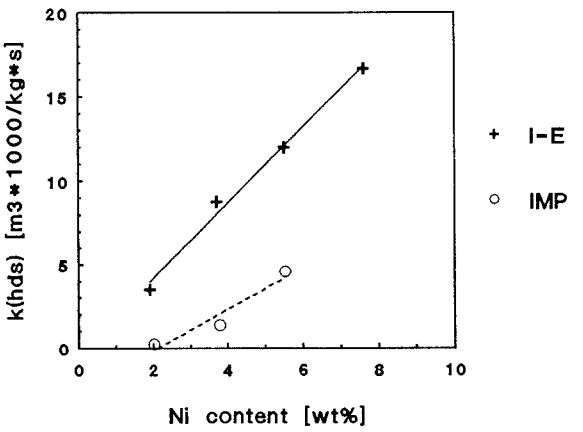

Fig. 8. Initial HDS activity of sulfided IMP and I-E NiNaY zeolites.

species. The more pronounced curvature found in the literature was explained by the paramagnetic effect of bare Ni^{2+} ions [1–3] which causes an adsorption factor (δ_{-1}) in eq. (1) which is larger than 1. The chemical shift plots (figs. 3–6) are almost linear in xenon density (the nonlinear adsorption term is very small), because the high electric field gradient of nickel is shielded by hydration (oxidic samples) or sulfidation (sulfided zeolites). The oxidic NiNaY samples studied by xenon NMR earlier by others [2,3] were dried under vacuum, and they are therefore different from the present samples. Traces of water or OH^- groups remained in the present samples, because they were evacuated only at room temperature.

Because of the high effective electric field gradient of bivalent Ni^{2+} cations (due to the unpaired electron) Xe atoms have a relatively long residence time on these ions [15]. Therefore, the chemical shifts are higher than in NaY zeolite without nickel, particularly at low Xe concentrations. This effect is seen from a shift higher than 59 ppm at zero Xe coverage (δ_0) for all NiNaY samples (table 2) and it is more evident on oxidic samples than on sulfided zeolites, because in the latter the nickel ions are presumably shielded by sulfur, which anion is more effective in shielding Ni^{2+} than the H_2O or OH^- groups, weakly adsorbed to the nickel ions.

The extrapolation of NMR chemical shift to zero xenon concentration (δ_0) gives information about the pore size and pore restrictions (hindrance of Xe diffusion) as well as intrinsic properties (e.g., polarity, Ni^{2+} concentration) of zeolites. In the case of nickel loaded zeolites higher nickel contents tend to deshield the ^{129}Xe NMR signal in two ways: increasing concentrations and/or decreasing void volumes. It is not known a priori to what extent both factors contribute to the NMR shift.

Essentially two kinds of empirical models are used to calculate the diameter of the supercage sphere (D) of faujasites from δ_0 [16], namely the Fraissard [7,8] and the Derouane [9–13] model. Neither of them can be applied in the present case [6], because these models do not take into account all of the effects contributing to the Xe NMR shift mentioned in the previous paragraph, especially the change in the composition of the zeolite cavities.

To deduce micropore volumes from xenon adsorption isotherm data is not straightforward since the packing of the large spherical Xe atom is poor [18], but some tendencies are remarkable. Two kinds of isotherm series are obtained in the present zeolite series. The isotherms of oxidic ion-exchanged zeolites are very similar to each other, while the adsorption capacity of the other samples decrease with increasing nickel loading.

Neither for the adsorption isotherm nor for the xenon NMR data a quantitative analysis is possible because of the earlier mentioned reasons. However, qualitative conclusions can be drawn. As follows from the very similar xenon adsorption isotherms (fig. 1) and adsorption heats (table 2) Ni^{2+} cation exchange of NaY zeolites does not seem to change essentially the micropore

volume of oxidic samples. At first sight this seems to be in contrast with the increasing zero extrapolated shifts with increasing nickel loading (fig. 7). This increase in δ_0 however may be mainly due to the increasing amount of the supercage surface covered by Ni^{2+} ions instead of Na^+ ions and is not necessarily due to the change of void volume available for xenon.

After sulfidation of ion-exchanged zeolites the resulting micropore volume decreases with increasing nickel content as follows from the decreasing adsorption capacities (fig. 1) and increasing xenon NMR chemical shifts extrapolated to zero xenon density (fig. 7). The changes in δ_0 are smaller in sulfided than in oxidic zeolites (fig. 7), because the xenon–sulfide interaction results in smaller shifts than the xenon–oxygen effect. As follows from the xenon NMR data the oxidic and sulfided nickel species are mainly located inside the supercages. Summarizing, it can be stated that the TPS and EXAFS results [5] point to a high degree of homogeneous sulfidation which is confirmed by narrow Xe NMR peaks (table 2), and there is no substantial migration of nickel sulfide from the supercages of NiNaY zeolites.

The zero extrapolated NMR shifts of oxidic samples prepared by impregnation (fig. 7) increase roughly linearly with increasing nickel loading and the increases in δ_0 are larger than in the case of their ion-exchanged counterparts. This means that the free volume available for xenon is smaller in the oxidic impregnated samples than in the corresponding oxidic ion-exchanged zeolites. In the former case the supercages contain a high amount of Na^+ ions and NiO species, while in the latter samples the amount of Na^+ ions is smaller, because the Na^+ ions are partially exchanged for hydrated Ni^{2+} ions or other $NiOH^+$ species.

The zero extrapolated chemical shifts of ^{129}Xe in sulfided IMP zeolites are practically identical (fig. 7) in contrast to their ion-exchanged and oxidic counterparts. However, the δ_0 values of the sulfided impregnated samples are much less than those of the corresponding sulfided ion-exchanged zeolites (except at 2% nickel loading). The xenon adsorption isotherms of the sulfided I-E and IMP samples are very similar at the same nickel loading (figs. 1 and 2), in spite of their different δ_0 shifts. Finally, also the hydrodesulfurization activity of IMP samples is significantly reduced (fig. 8). These observations can be explained by postulating a highly non-uniform distribution of the occluded $(NiS)_x$ particles in the sulfided impregnated zeolites. Some cavities are filled with nickel sulfide species (they practically block the entering of the xenon atoms), while others are empty.

The reason for the differences in catalytic activities between the ion-exchanged and impregnated samples (fig. 8) might be the decrease in the amount of the sulfide phase accessible to thiophene in the latter case compared to a larger amount of sulfide accessible in the more homogeneously dispersed ion-exchanged zeolites. Besides this dispersion effect it must be taken into account that sulfidation creates acidic sites in the ion-exchanged catalysts, which

might somehow influence the HDS reaction. Acid sites are also responsible for the strong deactivation of I-E samples [5].

5. Conclusions

The nickel species are located mainly inside the micropores of the zeolites in all samples. In the sulfided as well as the non-sulfided catalysts the distribution of the nickel species is more uniform in the ion-exchanged than in the impregnated samples. In the case of the sulfided zeolites prepared by impregnation we surmise that part of the nickel sulfide particles grow so as to fill the supercages. This explains their lower hydrodesulfurization activity compared to the ion-exchanged samples.

Acknowledgement

The authors thank Professor J. Fraissard and co-workers (University P. et M. Curie, France) and Professor J.B. Nagy (University Notre Dame de la Paix, Belgium) for very stimulating and helpful discussions. These investigations are supported in part by the Netherlands' Foundation for Chemical Research (SON) with financial aid from the Netherlands' Technology Foundation. The information included in this paper is partly derived from a contract (JOUF-0049 C) concluded with the European Economic Community.

References

[1] J. Fraissard and T. Ito, Zeolites 8 (1988) 350.
[2] A. Gedeon, J.L. Bonardet, T. Ito and J. Fraissard, J. Phys. Chem. 93 (1989) 2563.
[3] N. Bansal and C. Dybowski, J. Phys. Chem. 92 (1988) 2333.
[4] E.W. Scharpf, R.W. Crecely, B.C. Gates and C. Dybowksi, J. Phys. Chem. 90 (1986) 9.
[5] W.J.J. Welters, T.I. Korányi, V.H.J. de Beer and R.A. van Santen, in: *Proc. 10th Int. Congress on Catalysis*, Budapest 1992, in press.
[6] T.I. Korányi, L.J.M. van de Ven, W.J.J. Welters, J.W. de Haan, V.H.J. de Beer and R.A. van Santen, submitted.
[7] J. Demarquay and J. Fraissard, Chem. Phys. Lett. 136 (1987) 314.
[8] M. Springuel-Huet, J. Demarquay, T. Ito and J. Fraissard, Stud. Surf. Sci. Catal. 37 (1988) 183.
[9] E.G. Derouane, J.M. Andre and A.A. Lucas, Chem. Phys. Lett. 137 (1987) 336.
[10] E.G. Derouane and J.B. Nagy, Chem. Phys. Lett. 137 (1987) 341.
[11] E.G. Derouane, Chem. Phys. Lett. 142 (1987) 200.
[12] E.G. Derouane, J.M. Andre and A.A. Lucas, J. Catal. 110 (1988) 58.
[13] E.G. Derouane and M.E. Davis, J. Mol. Catal. 48 (1988) 37.

[14] A. Clark, *The Theory of Adsorption and Catalysis* (Academic Press, New York, 1970) p. 9.
[15] T. Ito and J. Fraissard, J. Chem. Soc. Faraday Trans. I 83 (1987) 451.
[16] Q.J. Chen and J. Fraissard, J. Phys. Chem. 96 (1992) 1809, 1814.
[17] T. Ito and J. Fraissard, J. Chem. Phys. 76 (1982) 5225.
[18] D.W. Johnson and L. Griffiths, Zeolites 7 (1987) 484.